Synthesis and Rigorous Analysis of Omnidirectional ADE Antenna with Shaped Main Reflector Described by Local Conic Sections

R. A. Penchel[1], S. R. Zang[2], and J. R. Bergmann[3]
CETUC, Pontifical Catholic University of Rio de Janeiro
Rio de Janeiro, RJ, Brazil, 22451-900
rapenchel@cetuc.puc-rio.br[1], sandro@cetuc.puc-rio.br[2], bergmann@cetuc.puc-rio.br[3]

F. J. S. Moreira
DELT, Federal University of Minas Gerais
Belo Horizonte, MG, Brazil, 31270-901
fernandomoreira@ufmg.br

***Abstract*—This work investigates the synthesis and analysis of omnidirectional dual-reflector antennas. The body-of-revolution subreflector is generated by a single conic section while the shaped main reflector is generated by a combination local conic sections, sequentially concatenated to each other. The main-reflector is shaped to radiate, under GO principles, a prescribed power density in the elevation. As case studies, four representative axis-displaced ellipse (ADE) configurations are synthesized to provide a sectoral coverage in the elevation plane. Two different ray structures are considered: with a real or a virtual main reflector caustic. For a rigorous analysis of the antenna, a hybrid technique based on Mode Matching and Method of Moments is employed.**

Keywords—Geometrical optics, reflector antenna, conic sections, hybrid tecnique.

I. Introduction

For services operating at frequency range from 10 to 66 GHz, compact single and dual reflector omnidirectional antennas can be employed in the hub station. For omnidirectional radiation patterns, Designs examples are found in the literature [1]–[3], where the reflector surfaces are bodies of revolution obtained by rotating the generating curves about a symmetry axis, as illustrated in Fig. 1. To ensure vertical polarization, the dual-reflector antenna designs can be fed by the coaxial TEM horn.

Several studies have dealt with the shaping of dual-reflector antennas for omnidirectional coverage by solving an ordinary differential equation derived from Geometrical Optics (GO) principles [1]–[2]. The shaping of dual-reflector antennas based on the combination of local conic sections has been investigated [4]. The concepts were further improved to treat arbitrary axisymmetric dual-reflector configurations [5] and omnidirectional dual-reflector arrangements [6,7]. Furthermore, the studies presented in [7] have been extended to design omnidirectional axis-displaced Cassegrain (OADC) antennas where the main reflector was shaped to provide the desired radiation pattern in the elevation plane. The present work extends the design procedure presented in [7] to shape the main-reflector of omnidirectional axis-displaced ellipse (OADE) antennas.

One of main objectives in design of these antennas is to produce very compact structures. However, the more compact is geometries, the greater is the coupling effects between feed and reflectors. To estimate the electromagnetic, a rigorous analysis is employed, where the Mode Matching Technique (MMT) is used to treat the fields inside the feed horn and the Method of Moments (MoM) to solve for the electromagnetic radiation [8]–[11].

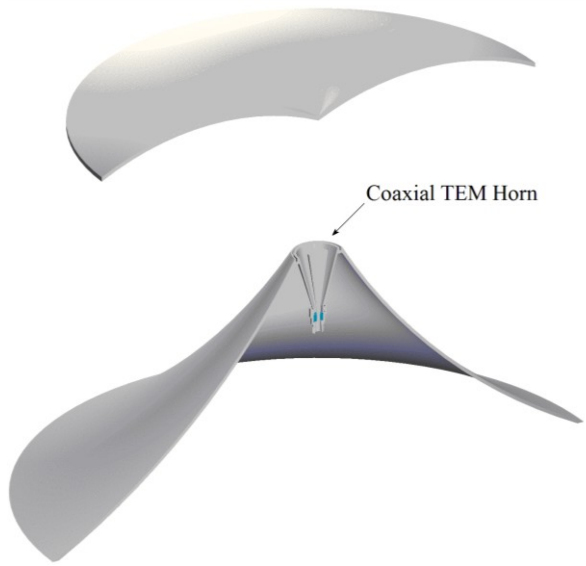

Fig. 1 – Circular symmetric reflector surfaces.

II. Synthesis Method

The GO shaping consists in determining the main reflector surface, which, given a spherical wave front with phase center at the origin (O) and circularly symmetric radiation pattern $G_F(\theta_F)$, provides the desired circularly symmetric radiation pattern $G_A(\theta)$ in its far-field region. The shaped main reflector has its generatrix described by local conic sections sequentially concatenated (see Fig. 2). The subreflector is generated by a known conic section, determined with the help of the formulation in [3]. The subreflector conic section has two foci: one at the origin (O) and the other at the point P, which defines the subreflector real annular caustic after the conic section is rotated about the z-axis (see Fig. 2).

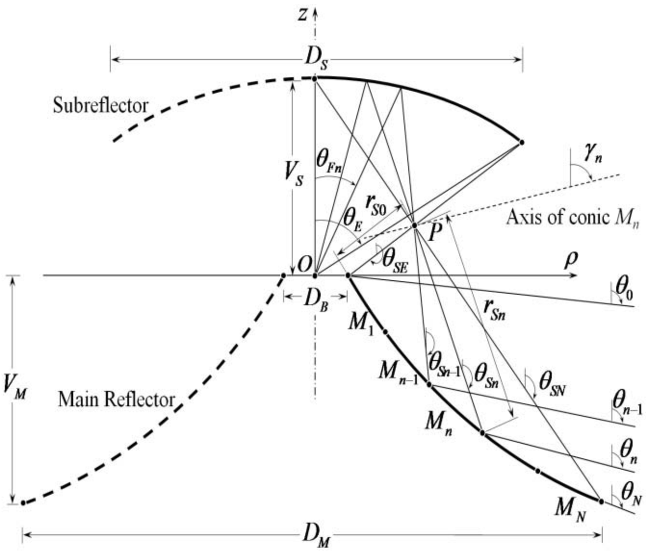

Fig. 2 – Conic sections representing the generatrix shaped main reflector.

The shaped main reflector generatrix is composed by a combination of local conic sections M_n (n = 1,…, N) sequentially concatenated, all of them with one of their focci at P. In order to uniquely determine each one of main-reflector conic sections M_n, three parameters must be determined: the inter-focal distance ($2c_n$), the eccentricity (e_n), and the angle γ_n of the conic axis. So, a set of three equations must be found for each step n of the iterative process [7]. The first equation is given by polar conic equation applied to each one of n conic section M_n. The second equation, which is an angular relation between $\theta_S = \theta_{Sn}$ (the ray direction before reflection at M_n) and $\theta = \theta_n$ (the ray direction after reflection, toward the far-field region), is obtained by imposing Snell's Law at M_n. The third equation is obtained from the same angular relation, but for the optical ray of the previous step (i.e., $\theta_S = \theta_{Sn\text{-}1}$ and $\theta = \theta_{n\text{-}1}$) [7]. So, with a set of three equation for each iterative step n, one is capable of determining the necessary conic parameters and, consequently, M_n.

To solve the set of linear equations, one must find the direction θ_n. By enforcing the conservation of energy along the tube of rays departing from O toward the main-reflector far-field region, one obtains the integral form of the mapping equation, which can be solved numerically [7]. The iterative process starts at $n = 0$, with $\theta_{F0} = \theta_E$ (θ_{SE} is obtained from θ_E with the help of the subreflector conic equation), $\theta = \theta_0$, and r_{S0} given by the location of the subreflector caustic P and by the desired diameter D_B of the main-reflector central opening (see Fig. 2).

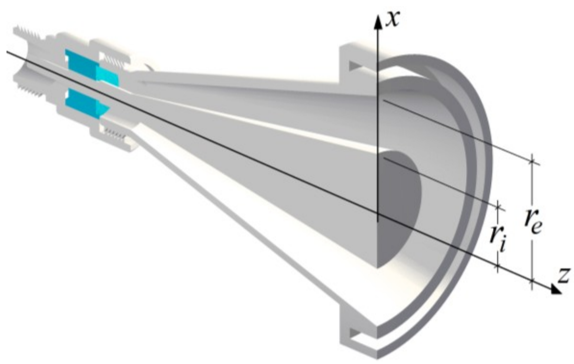

Fig. 3 – Coaxial TEM horn.

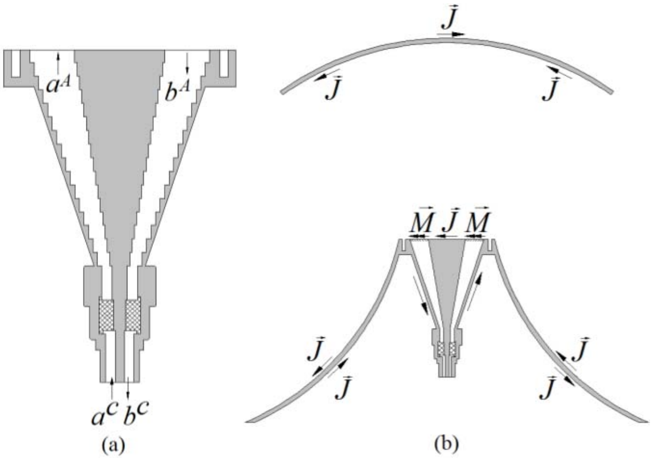

Fig. 4 – (a) Coaxial horn represented as series of stepped waveguides and (b) MoM model of the exterior surface currents (feed and reflectors).

III. ANALYSIS METHOD

In the analysis scheme, the coaxial horn (see Fig. 3) is represented as series of stepped coaxial waveguides sections (see Fig. 4.(a)) and the Mode Matching technique is performed by rigorously enforcing the boundary conditions at each step, including the coaxial connector and coupling structure with dielectric loaded. It results in a scattering matrix for the entire transition region that depends on the geometrical parameters and on the wavelength as well as the number of higher modes considered to ensure continuity of the electric and magnetic fields throughout the transition region. Considering the TEM fundamental mode as the only incident mode at connector region C and the circularly symmetric structure, only the TEM and TM are excited throughout the entire transition region, as the TE mode do not couple with the TEM excitation.

Part of the power of the modes reaching the aperture (region A) is radiated into the space that will induce surface currents on the surface reflectors (see Fig. 4.(b)), while the rest is guided back into the horn. The interaction between these fields in the coaxial horn interior region and the reflectors exterior current contributions is accurately analysed by using the EFIE on the exterior surfaces of the coaxial horn. The equivalence currents principle is introduced to formulate the HFIE on the radiating aperture which combines the interior field transition problem with the exterior radiation. The procedure is similar to those described in [8]–[9]. Here, the procedure is adapted to include the reflectors and a coaxial feed horn excited by the TEM mode.

As described in [9], the MoM is employed to solve the EFIE and MFIE in order to calculate the radiate fields and the amplitude of the reflected modes $[b^A]$ into the horn. To apply the above strategy, an equivalent to the actual electromagnetic problem is defined by replacing the feed radiating aperture by a sheet of perfect conductor with an equivalent magnetic current density $\vec{M}$ (see Fig. 4.(b)). The magnetic current density radiates into the space and induces an electric surface current $\vec{J}$ on the metallic wall of the equivalent problem. These currents ensure the continuity of the tangential magnetic field across the aperture and zero tangential electric field on the metallic surface at the aperture and reflectors.

To apply the MoM solution, the current densities $\vec{M}$ and $\vec{J}$ are expanded by sub sectional roof-top patch modes and, particularly, over the aperture this functions are converted into eigenmodes of the aperture fields. The application of the MoM analysis technique yields the antenna radiation pattern as well as the antenna return loss at the end of the *N*-type connector.

To apply the above strategy, an equivalent to the actual electromagnetic problem is defined by replacing the feed radiating aperture by a sheet of perfect conductor with an equivalent magnetic current density (Fig. 4.b). In the MoM scheme, the electric and magnetic current densities are expanded by sub-sectional roof-top patch modes and, particularly, over the aperture this functions are converted into eigenmodes of the aperture fields. The application of the MoM technique yields the antenna radiation pattern as well as the antenna return loss at the end of the *N*-type connector.

IV. STUDY CASES

To illustrate the shaping technique described in the Sect. II, four case studies are presented. The first two examples are designed to provide a sectoral coverage in the elevation plane over ±7.5° with respect to the horizon with real (Case A.I) or virtual (Case A.II) main-reflector caustic in the elevation plane. The last two cases provide sectoral coverage over ±15° with respect to the horizon with real (Case B.I) or virtual (Case B.II) main-reflector caustic. The feed is assumed to be a TEM coaxial horn (see Fig. 3) which the function that describes the radiation pattern in the far-field region is given by [2]:

$$G_F(\theta_F) = G_{0F}\left[\frac{J_0(kr_i\sin\theta_F) - J_0(kr_e\sin\theta_F)}{\sin\theta_F}\right]^2 \qquad (1)$$

where G_{0F} is a normalization factor. The internal and external aperture radii are $r_i = 0.45\lambda$ and $r_e = 0.90\lambda$, respectively. The objective function that describes the constant sectoral radiation pattern of the dual-reflector antenna in the elevation plane is given by [7]:

$$G_A(\theta) = \frac{1}{2\pi}\left|\frac{1}{\cos\theta_1 - \cos\theta_2}\right| \qquad (2)$$

which has been normalized for unit radiated power.

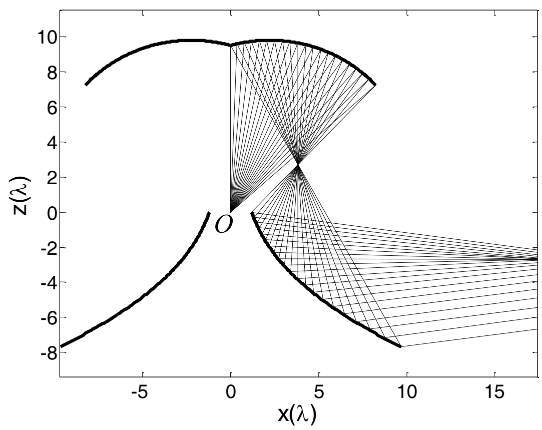

Fig. 5 – Generatrices of a shaped OADE dual-reflector antenna (Case A.I) with a real main-reflector caustic in the elevation plane.

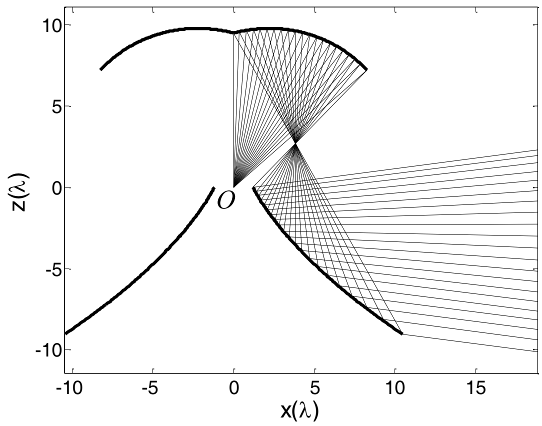

Fig. 6 – Generatrices of a shaped OADE dual-reflector antenna (Case A.II) with a virtual main-reflector caustic in the elevation plane.

A. OADE Configuration for Sectoral Coverage over ±7.5 °

In the first case study (Case A.I), the main reflector of an OADE configuration was synthesized to radiate, under GO principles, a sectoral illumination in the elevation plane over ±7.5° with respect to the horizon (i.e., from $\theta_0 = 97.5°$ to $\theta_N = 82.5°$). As $\theta_0 > \theta_N$, the main reflector has a real caustic in the elevation plane (see Fig. 5). The subreflector generating ellipse was determined from a classical OADE configuration with the following parameters (see Fig. 2): $V_S = 9.5\lambda$, $D_B = 2.4\lambda$, main-reflector projected diameter $D_M = 20\lambda$, focus *O* at the plane of the main-reflector central opening ($z_B = 0$), main-reflector aperture width $W_A = 8.25\lambda$, and $\gamma = 90°$. These values provide an ellipse with an eccentricity equal to 0.270899, an inter-focal distance $2c = 4.69\lambda$, and an axis with a tilt angle of 54.79° with respect to the *z*-axis. As a consequence, the projected diameter of the subreflector $D_S = 16.49\lambda$ and the subreflector edge angle $\theta_E = 48.72°$. These parameters also provide $r_{S0} = 3.77\lambda$ as an initial value for the shaping procedure presented in Sect. II. The generatrices of the subreflector and shaped main reflector are illustrated in Fig. 5.

In the second example (Case A.II), the subreflector is the same one used in Case A.I. The main reflector was shaped with an inverted far-field angular limits in the elevation plane (i.e., from $\theta_0 = 82.5°$ to $\theta_N = 97.5°$). As $\theta_N > \theta_0$, the main reflector now has a virtual caustic in the elevation plane (see Fig. 6). Some important dimensions of the shaped main reflector of Cases A.I and A.II are listed in Table I.

TABLE I

PARAMETERS	CASE A.I	CASE A.II	CASE B.I	CASE B.II
D_M (λ)	19.35	20.89	18.89	22.16
V_M (λ)	7.68	9.04	7.26	10.17
VOLUME($\lambda^3 10^3$)	4.2999	5.0105	4.1002	5.6606

The shaping procedure discussed in Sect. II is simpler than those based on the evaluation of an ordinary differential equation, like that adopted in [2]. It also has a faster numerical convergence, providing the same precision of the procedure based on the solution of a differential equation with approximately 100 times less steps, as reported in [7]. To illustrate this feature, the main-reflector RMS error (with respect to a reflector shaped with a very large N value) obtained by the present technique and that of [2] are depicted in Fig. 7 as a function of log(1/N) for Cases A.I and A.II. The RMS behavior of both (real or virtual caustic) cases are basically the same and also the same of OADC axis-displaced configuration [7].

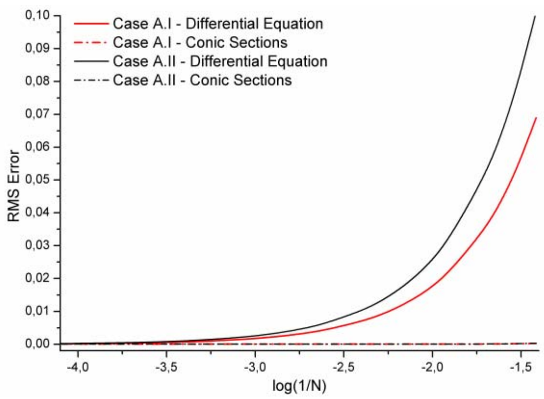

Fig. 7 – Main-reflector RMS error with respect to N for Cases A.I and A.II.

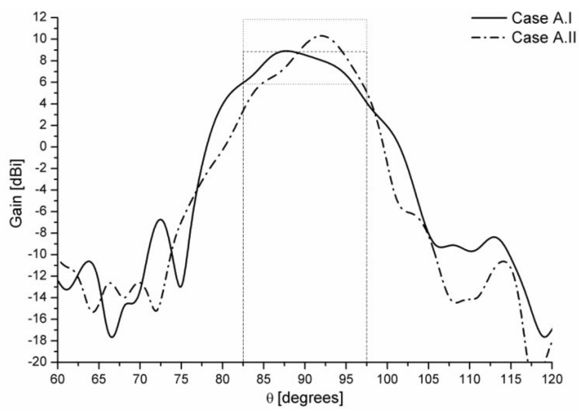

Fig. 8 – MoM radiation patterns (Cases A.I and A.II) in the elevation plane.

The radiation patterns of Cases A.I and A.II were simulated by the method of moments (MoM) technique and are illustrated in Fig. 8, together with the prescribed GO far-field pattern of (2), used for the main-reflector shaping. As we can note, both results are close to the object function. The Differences observed can be attributed to diffractions effects and electromagnetic coupling not considered by the synthesis. The Fig. 9 shows the return loss obtained from the MoM analysis for shaped dual-reflector antenna and for the feed horn.

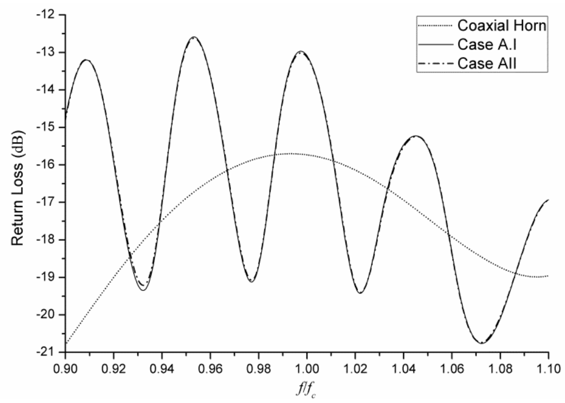

Fig. 9 – Feeder and antenna return loss for Cases A.I and A.II

B. OADE Configuration for Sectoral Coverage over ±15°

The omnidirectional ADE configuration of Case B.I was designed to radiate, once again, a sectoral illumination in the elevation plane but over a wider range (±15° with respect to the horizon, (i.e., from $\theta_0 = 105°$ to $\theta_N = 75°$). The subreflector is the same of Cases A.I and A.II. The generatrices of the subreflector and shaped main reflector are illustrated in Fig. 10, where the real caustic of the main reflector is apparent. In last case study (Case B.II), the subreflector was kept the same of previous cases, and angular limits of far-field were inverted(i.e., from $\theta_0 = 75°$ to $\theta_N = 105°$). As $\theta_N > \theta_0$, the main reflector now has a virtual caustic in the elevation plane (see Fig. 11). Once again, the antenna with a real main-reflector caustic presented a smaller volume, as can be inspected from Table I for Cases B.I and B.II. The radiation patterns of Cases B.I and B.II were simulated by the MoM and are illustrated in Fig. 12, together with the prescribed GO far-field pattern.

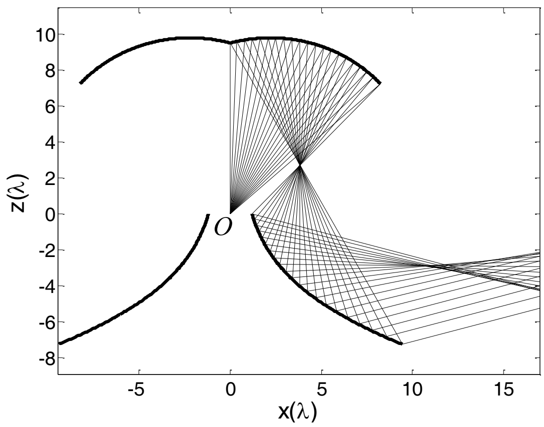

Fig. 10 – Generatrices of the shaped OADE dual-reflector antenna (Case B.I) with a real main-reflector caustic.

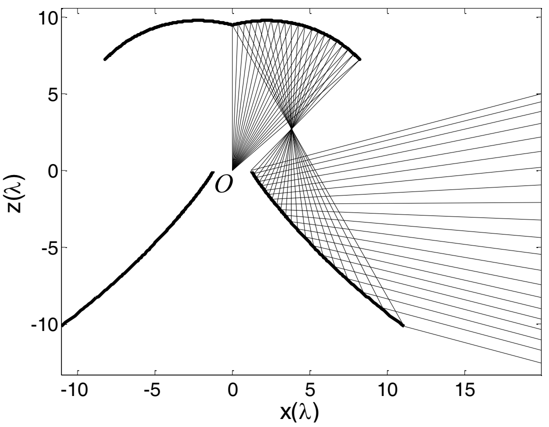

Fig. 11 – Generatrices of the shaped OADE dual-reflector antenna (Case B.II) with a virtual main-reflector caustic.

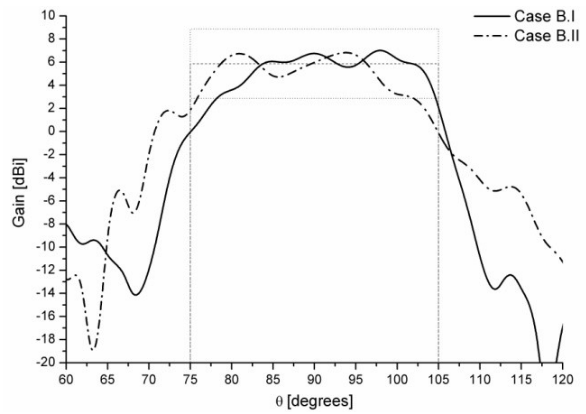

Fig. 12 – MoM radiation patterns (Cases B.I and B.II) in the elevation plane.

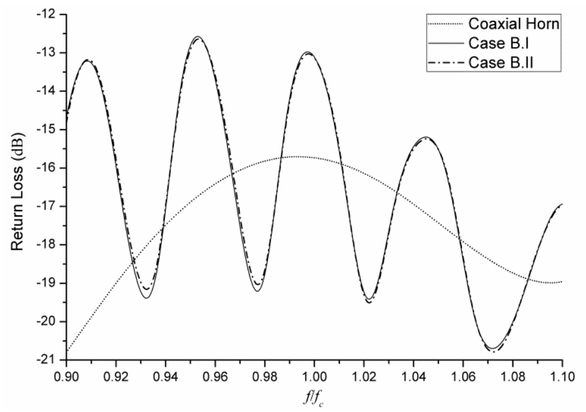

Fig. 13 – Feeder and antenna return loss for Cases B.I and B.II.

The Fig. 13 shows the return loss obtained from the MoM analysis for shaped dual-reflector antenna and for the feed horn.

Comparing cases studies A and B we can note that when the desired sectoral illumination is attained for a wider angular range the radiation pattern is closer to the objective function than the in the narrower case. We can also observe (Fig. 12) that for Case B.I the gain moves further away from the objective region between $\theta = 75°$ and $80°$ and for Case B.II it occurs between $\theta = 100°$ and $105°$. This happens because the subreflector has a lower illumination in regions close to $\theta_F = 0$, as the feeder has a null radiation in this direction

I. Conclusions

This work presented a method for the GO synthesis of omnidirectional dual-reflector antennas. The procedure shapes the main-reflector generatrix, which is represented by local conic sections consecutively concatenated. The subreflector is not shaped and its generatrix is represented by a single conic section. It was shown that the present technique is much more accurate than the one present in [2].

A full-wave analysis was conducted to validate the shaping procedure and measure electromagnetic effects between coaxial horn and the omnidirectional dual-reflector system. The analysis algorithm was applied to calculate the antenna radiation pattern and the antenna return loss of the projected antenna.

Acknowledgment

This work was supported in part by CNPq, Brazil, under Projects 470699/2006-0 and 310945/2006-2.

References

[1] A. P. Norris and W. D. Waddoup, “A millimetric wave omnidirectional antenna with prescribed elevation shaping,” in Proc. ICAP—4th Int. Conf. Antennas and Propagation, 1985, pp. 141–145.

[2] J. R. Bergmann and F. J. S. Moreira, “Omnidirectional ADE antenna with GO shaped main reflector for arbitrary far-field pattern in the elevation plane,” IET Microwaves, Antennas & Propagation, vol. 3, no. 5, pp. 1028-1035, Oct. 2009.

[3] F. Moreira and J. Bergmann, "Axis-displaced dual-reflector antennas for omnidirectional coverage with arbitrary main-beam direction in the elevation plane," *IEEE Trans. Antennas Propagat.*, vol. 54, no. 10, pp. 2854—2861, Oct. 2006.

[4] Y. Kim and T.-H. Lee, “Shaped circularly symmetric dual reflector antennas by combining local conventional dual reflector systems,” *IEEE Trans. Antennas Propagat.*, vol. 57, no 1, pp. 47—56, Jan. 2009.

[5] F. Moreira and J. Bergmann, “Shaping axis-symmetric dual-reflector antennas by combining conic sections," *IEEE Trans. Antennas Propagat.*, vol. 59, no. 3, pp. 1042—1046, March 2011.

[6] F. Moreira and J. Bergmann, “Omnidirectional dual-reflector shaping by concatenating conic sections,” 4th European Conference on Antennas and Propagation (EuCAP 2010), Barcelona, Spain, April 2010.

[7] R. Penchel, J. Bergmann, and F. Moreira, “An omnidirectional dual-reflector antenna with a shaped main reflector described by local conic sections,” 5th European Conference on Antennas and Propagation (EuCAP 2011), Rome, Italy, pp. 1221—1224, April 2011.

[8] E. Kuhn and V. Hombach, “Computer-aided analysis of corrugated horns with axial or ring-loaded radial slots”, Proc. ICAP 83, Part 1, pp.127-131, 1983.

[9] K. Lui, C. Balanis, C. Birtcher, and G. Barber, “Analysis of pyramidal horn antennas using moment methods”, *IEEE Trans. Antennas Propagat.*, vol. 41, no. 10, pp. 1379–1389, Oct. 1993.

[10] S. R. Zang, J. R. Bergmann, and F. J. S. Moreira, “Omnidirectional Dual-reflector Antenna with a GO Shaped Main Reflector for an Arbitrary Far-Field Pattern in the Elevation Plane,” *3rd European Conference on Antennas and Propagation (EuCAP 2009)*, Berlin, Germany, pp. 3047—3050, March 2009.

[11] J. R. Mautz and R. F. Harrington, “An Improved E-Field Solution for a Conducting Body of Revolution,” Technical Report TR-80-1, Dept. Electrical and Computer Engineering, Syracuse University, 1980.